

Multiscale analysis of turbulence-flame interaction based on measurements in premixed flames

Chantriaux, François; Quenouille, Théo; Doan, Nguyen Anh Khoa; Swaminathan, Nedunchezian; Hardalupas, Yannis; Taylor, A. M.K.P.

DOI

[10.1016/j.combustflame.2022.111982](https://doi.org/10.1016/j.combustflame.2022.111982)

Publication date

2022

Document Version

Accepted author manuscript

Published in

Combustion and Flame

Citation (APA)

Chantriaux, F., Quenouille, T., Doan, N. A. K., Swaminathan, N., Hardalupas, Y., & Taylor, A. M. K. P. (2022). Multiscale analysis of turbulence-flame interaction based on measurements in premixed flames. *Combustion and Flame*, 239, Article 111982. <https://doi.org/10.1016/j.combustflame.2022.111982>

Important note

To cite this publication, please use the final published version (if applicable).
Please check the document version above.

Copyright

Other than for strictly personal use, it is not permitted to download, forward or distribute the text or part of it, without the consent of the author(s) and/or copyright holder(s), unless the work is under an open content license such as Creative Commons.

Takedown policy

Please contact us and provide details if you believe this document breaches copyrights.
We will remove access to the work immediately and investigate your claim.

Abstract

Multi-scale analysis of turbulence–flame interaction is performed using experimental data sets from three methane- and propane-fired premixed, turbulent V-flames, at an approach flow turbulent Reynolds number of 450 and a ratio of r.m.s. fluctuating velocity from the mean to laminar flame speed of between 2.1 and 3.0, straddling the border between corrugated flamelets and thin reaction zone in the Borghi-Peters diagram. The measurements were made in the plane of a single laser sheet using stereo particle image velocimetry SPIV and planar laser-induced fluorescence to measure three orthogonal components of velocity and flame OH. Methods to approximate the remaining, unmeasured, out of plane derivatives are described. The instantaneous SPIV images were bandpass filtered at user-specified characteristic length scales L_ω and L_s (for vorticity and strain rate, respectively) resulting in instantaneous bandpass-filtered velocity fields, $\underline{u}_b^{L_\omega}$ and $\underline{u}_b^{L_s}$, which were further analysed to give the bandpass filtered vorticity field, $\underline{\omega}^{L_\omega} = \nabla \times \underline{u}_b^{L_\omega}$, the strain-rate field, $e_{ij}^{L_s}$, and the tangential strain rate field $a_T^{L_s}$.

This work quantifies two aspects of turbulence-flame interaction. The first aspect is that of the flame interaction of eddies of size L_s on the turbulence, as found by the statistics of the alignment of vorticity with strain rate. We find that vortical eddies with scale about $L_\omega = 2\delta_{th}$ (where δ_{th} is the flame thickness,) are stretched by L_s structures which are larger than about $2 L_\omega$, with this factor broadly true also for vortical eddies of scales $L_\omega = 4\delta_{th}$ and $L_\omega = 6\delta_{th}$. Within the limitations of the data set, these findings are consistent with those in the literature on reacting and non-reacting flows, suggesting that the premixed flame has had little influence on the vortex stretching mechanism.

The second aspect of turbulence-flame interaction examined is that of flame surface-averaged tangential strain rate imparted by eddies. Eddies with length scales L_s smaller than $2\delta_{th}$ have the strongest individual contribution but eddies of this length scale and smaller contribute only about 1/3 of the total tangential strain rate. This is larger than the 10 % that has been reported in the literature based on analysis of DNS predictions of premixed flames at turbulent Reynolds numbers up to 110. Eddies with length scale L_s larger than about $20\delta_{th}$ contribute a negligible amount to the total tangential strain rate. We have found no evidence that the Lewis number up to about 1.8 has an observable effect, but this may reflect the inability of the current instruments to resolve vortical structures down to $L_\omega = \delta_{th}$. In the context of large eddy simulations (LES) of premixed combustion, these results are preliminary experimental evidence into the suggestion that resolving turbulence scales down to a few multiples of δ_{th} might be adequate to capture much of the flame straining caused by turbulence.

1
2
3 Multiscale analysis of turbulence-flame interaction based on
4
5 measurements in premixed flames
6
7

8 François Chantriaux^a, Théo Quenouille^b, Nguyen Anh Khoa Doan^c, Nedunchezian
9 Swaminathan^d, Yannis Hardalupas^e, A M K P Taylor^{e,*}
10

11
12 ^a*Ecole Polytechnique, Palaiseau, France*

13
14 ^b*ENSTA Paris, Institut Polytechnique de Paris, Palaiseau, France*

15
16 ^c*Faculty of Aerospace Engineering, Technical University of Delft, Kluyverweg 1, 2629 HS Delft, The*
17 *Netherlands*

18
19 ^d*Department of Engineering, University of Cambridge, Trumpington Street, Cambridge CB2 1PZ, United*
20 *Kingdom*

21
22 ^e*Thermofluids Division, Department of Mechanical Engineering, Imperial College London, London SW7 2BX,*
23 *United Kingdom*
24
25

26
27 *Keywords:* Stereo particle image velocimetry; laser induced planar fluorescence; Turbulent
28 premixed flame; Flame-turbulence interaction; Multiscale decomposition; Flame tangential
29 strain rate
30
31

32 33 34 Nomenclature

35 36 Latin Letters

37
38
39 a_T the tangential strain rate

40
41 c reaction progress variable

42
43 c_m a constant determined from the ratio of moments of the probability density distribution
44 of c
45

46
47 D Diffusivity of c

48
49 D_f fractal dimension, $D_f = -\log(4)/\log(R_l)$

50
51 Da Damköhler number

52
53 e_{ij} strain rate tensor $0.5(\partial u_i/\partial x_j + \partial u_j/\partial x_i)$

54
55 K_2 a constant $K_2 = 1/(2c_m - 1)$

56
57 K_m is flame curvature, $\partial n_i/\partial x_i$

58
59 Ka Karlovitz number

60
61 *Corresponding author

62 *Email address:* a.m.taylor@imperial.ac.uk (A M K P Taylor)
63

1	
2	
3	L length scale of bandpass filter
4	
5	L_s the considered lengthscale of the rate of strain field after bandpass filtering
6	
7	L_ω the considered lengthscale of the vorticity field after bandpass filtering
8	
9	L_{max} maximum PIV lengthscale = $21 \min(N_i \cdot \rho, N_j \cdot \rho)$
10	
11	Le Lewis number
12	
13	N_i, N_j PIV velocity field resolution in i and j coordinate directions
14	
15	n_i the component of \underline{n} in the x_i direction
16	
17	Re_T Reynolds number based on turbulence
18	
19	s_L flame propagation speed in the normal direction
20	
21	t time
22	
23	u'_1 characteristic fluctuating velocity; or axial r.m.s. velocity measured by hot wire anemometry
24	
25	u_i Components of velocity vector
26	
27	x_i Cartesian coordinate system. Axis of the stabilising wire runs along the x_3 coordinate
28	

Greek Letters

29	
30	
31	δ_{ij} The Kronecker symbol
32	
33	δA the change of elemental flame area
34	
35	δ_{th} the Laminar flame thickness
36	
37	κ flame stretch = $\frac{1}{\delta A} \frac{d\delta A}{dt}$
38	
39	Λ the integral length scale of the turbulent flow
40	
41	λ Taylor microscale
42	
43	ν kinematic viscosity
44	
45	ξ a test
46	
47	ρ density
48	
49	τ heat release parameter $\frac{T_b - T_u}{T_u}$ with T_b, T_u the temperature of the burned and unburned gases respectively
50	
51	ϕ equivalence ratio
52	
53	$\bar{\chi}$ scalar dissipation rate
54	
55	$\bar{\omega}$ $K_2 \bar{\chi}$, time-averaged chemical reaction rate
56	
57	
58	
59	
60	
61	
62	
63	
64	
65	

1. Introduction

Bray [1] laid out, in a paper published more than four decades ago, an exposition of "The interaction between turbulence and combustion". A seminal result was to show that in the limit of large fluctuations, as exist in most turbulent premixed flames, combustion is controlled by turbulent mixing

$$\bar{\omega} = K_2 \bar{\chi} \quad (1)$$

$$\bar{\chi}_i \equiv 2\rho D \frac{\partial c''}{\partial x_k} \frac{\partial c''}{\partial x_k} \quad (2)$$

where $\bar{\omega}$ is the time-averaged chemical reaction rate; $K_2 = 1/(2c_m - 1)$ where c_m is determined from the ratio of moments of the probability density distribution of c which is a reaction progress variable; $\bar{\chi}$ is the time-averaged scalar dissipation rate of c ; and the double prime denotes fluctuation from the Favre-average. The equation is derived under benign assumptions and with the physical insight that '...the mixture is made up of packets of burnt and unburnt gas, separated by narrow reaction zones...'. Bray notes that a '...powerful description of the premixed turbulent flame with arbitrarily complex chemistry can be developed ... if combustion is assumed to occur only in laminar flamelets of known structure...For the ... description to be valid, *turbulence must not distort the laminar flamelet structures sufficiently to influence the assumed relationship between composition and temperature...*' (our emphasis). The current contribution concerns itself, experimentally, with this interaction between combustion and turbulence [2] in premixed flames, manifested as the 'distortion' associated with the wrinkling and straining of the flame which are caused, respectively, by the vorticity- and strain- dominated structures in turbulence.

Wrinkling and stretching produce flame stretch, as quantified by fractional changes in its elemental surface area δA ([3]):

$$\kappa = \frac{1}{\delta A} \frac{d\delta A}{dt} = (\delta_{ij} - n_i n_j) e_{ij} + s_d \frac{\partial n_i}{\partial x_i} = a_T + s_d K_m \quad (3)$$

where δ_{ij} is the Kronecker symbol; $\underline{n} = -\nabla c/|\nabla c|$ is the flame normal vector, found from the reaction progress variable c ; n_i is the component of \underline{n} in the x_i direction; $e_{ij} = 0.5(\partial u_i/\partial x_j + \partial u_j/\partial x_i)$ is the strain tensor with u_i being the turbulent velocity component in the direction i ; and $s_d = (Dc/Dt)/|\nabla c|$ is the displacement speed, [4]. The last equation on the right summarises the effect of stretch in terms of tangential strain rate, a_T , and curvature, $K_m = \nabla \cdot \underline{n}$, which arise from straining and wrinkling. Qualitatively, low to moderate stretch rate creates active flame surface: in contrast, too high a stretch rate might result in the flame being quenched.

The flame stretch appears in several approaches for turbulent combustion modelling and calculation, including in the 'flame surface density' description as a source for flame surface area [5, 6], where the surface averaged stretch can be negative [7, 8, 9] and in LES for the thickened flame model [10, 11, 12] and in the 'G equation' approach [12] For both Reynolds Averaged Navier-Stokes (RANS) [13, 14] and LES [10, 11] calculations of premixed combustion, proposals include the 'strained flamelets' approach and the use of an 'efficiency (correction) function'. These approaches work well for RANS calculations and, for LES calculations which resolve

1
 2
 3 most of the dynamic scales, there may be no need to try to account for the effect of sub-grid
 4 eddies, because these eddies may be too weak to stretch the flame. [14], by modelling the
 5 tangential strain rate acting on flame surfaces in RANS, introduced this efficiency function.
 6 It was derived by combining turbulence theory and DNS results to account for the fact that
 7 the strain generated by the vortex (*i.e.* the rate of strain $(r/\delta_{th}) \cdot (v_r/r)$ induced by a vortex
 8 dipole of characteristic velocity and length scale v_r and r) is not entirely converted into effective
 9 flame stretch (*i.e.* $(1/A)(dA/dt)$). This function mainly reduces or eliminates the influence of
 10 smallest turbulent motions (*i.e.* smaller than size of the order of few flame thickness), which
 11 are found to be unable to wrinkle the flame front. This work was subsequently extended to
 12 LES, and further developed by [10, 11, 15, 16]. On the basis of experiments, however, [17], [18]
 13 concluded that not only was an interaction between a vortex pair and a planar flame surface
 14 comparatively rare, but also that the straining and wrinkling of the flame surface were not well
 15 characterised by the vortical structures. Instead, straining and wrinkling were generally caused
 16 by large groups of multiply curved and intertwined structures. In addition, they found that
 17 stretch-efficiency functions developed from simplified vortex-flame interactions substantially
 18 over-predict the measurements.
 19
 20
 21
 22
 23

24 Be that as it may, the efficiency function correctly highlights what might be expected, namely
 25 that length scales larger than the flame thickness can stretch the flame more ‘efficiently’ than do
 26 small scales. In this context, [19, 20] concluded that the Kolmogorov scales had lower efficiency
 27 for flame stretching; [21, 22] in contrast, suggested that this scale produced the highest stretch.
 28 [22, 23] suggested the Taylor timescale to be an appropriate scaling factor for the tangential
 29 strain rate but thermo-diffusive instabilities may affect the flame-turbulence interaction in these
 30 hydrogen- air flames. Such contradictory views raised two questions, namely (1) what is the
 31 smallest turbulence scale imparting significant flame stretch and (2) what is the implication for
 32 modelling of filtered reaction rate in LES? As already stated, the flame wrinkling and straining
 33 are caused, respectively, by the vorticity- and strain- dominated structures in turbulence. In
 34 turn, the vortical structures are produced by the vortex stretching mechanism in turbulence
 35 and hence the influence of the turbulence-flame interaction on this mechanism also becomes of
 36 interest.
 37
 38
 39
 40

41 To answer these questions, [24] analysed five premixed flames generated by Direct Numerical
 42 Simulation (DNS), spanning from the corrugated-flamelet to the thin reaction zones in the
 43 regime diagram of Peters. They analysed the instantaneous velocity field by educing turbulent
 44 eddies of various sizes using the multiscale analysis called bandpass filtering [25] which filters
 45 out scales smaller than the specified one, and larger ones less sharply: the analysis is briefly
 46 described in subsection 2.4.1. This allowed the construction of filtered rate-of-strain fields,
 47 $e_{ij}^{L_s}$, and filtered vorticity fields, $\underline{\omega}^{L_\omega} = \nabla \times \underline{u}_b^{L_\omega}$ (where L_ω and L_s refer to the length scales
 48 chosen to filter the vorticity and strain rate fields). The intensity of vorticity of the velocity field
 49 which is bandpassed at length L_ω is quantified in terms of the filtered enstrophy field $0.5|\underline{\omega}^{L_\omega}|^2$.
 50
 51
 52

53 In terms of flame wrinkling, the results show that downstream of the flame there are fewer small
 54 scale vortical structures (in terms of the enstrophy structures at length scale L_ω comparable
 55 to the flame thickness structures), confirming that a flame dampens turbulence, as might be
 56 expected. Nevertheless, the influence of the flame on the mechanism of vortex stretching, and
 57 the role of relative eddy sizes on this mechanism, were not unduly influenced by the presence
 58 of chemical reactions and heat release. These conclusions were established by investigating the
 59 vortex stretching mechanism which produces enstrophy at scale L_ω due to straining structures at
 60
 61
 62
 63
 64
 65

scale L_s , namely $\omega_i^{L_s} \omega_j^{L_s} e_{ij}^{L_s} = |\underline{\omega}^{L_s}|^2 (\alpha^{L_s} \cos^2 \theta_\alpha + \beta^{L_s} \cos^2 \theta_\beta + \gamma^{L_s} \cos^2 \theta_\gamma)$ where α^{L_s} , β^{L_s} and γ^{L_s} are the principal components of $e_{ij}^{L_s}$ with $\alpha^{L_s} > \beta^{L_s} > \gamma^{L_s}$ and the θ_i are the corresponding angles between the vorticity vector and these principal components. The alignment between the vorticity vector, $\underline{\omega}$, and the principal components of strain rate tensor, was similar to the non-reacting flow results in [25], namely that there is a preferential alignment of $\underline{\omega}$ with α from eddies larger than the vortical structure and the alignment with β is approached when L_s is less than or equal to L_ω . Specifically, the peak probability of $0.98 \leq |\cos \theta_\alpha| \leq 1$ as a function of L_s/L_ω occurred between 3 and 4 for the flames, implying that the vortical structure is stretched mostly by structures 3 to 4 times bigger than itself.

In terms of tangential strain rate, their results suggested that eddies in the range $3 \leq L_s \leq 17$ have substantial effect on flame straining, while eddies smaller than $3 \delta_{th}$, and eddies larger than $17 \delta_{th}$, contributed less than 20 % and 10 % to the total tangential strain rate respectively. This was established by investigating the fractional contribution of eddies of scale L_s to the tangential strain rate $a_T^{L_s} = (\delta_{ij} - n_i n_j) e_{ij}^{L_s}$ as

$$\widehat{\psi}(L_s^+) = \psi(L_s^+) / \psi_{int} \quad (4)$$

where $\psi(L_s^+)$ is a surface-averaged value $\langle |\nabla c| a_T^{L_s^+} \rangle / \langle |\nabla c| \rangle$ and $L_s^+ = L_s / \delta_{th}$ is the normalised bandpass filtered scale with $\psi_{int} = \int_0^\infty \psi dL_s^+$ being the surface-averaged contribution coming from all eddies in the flow. It was concluded, by examining four length scales (‘Roberts’, [20], Gibson, a length scale corresponding to the peak surface-averaged tangential strain rate and a length scale below which eddies contribute 10 percent or smaller to the total tangential strain rate) that the range of eddies having weak influence on straining the flame is larger than that originally thought. The significance is that this implies that resolving turbulence scales down to a few multiples of δ_{th} would be enough to capture most of the flame straining caused by turbulence. These scales can be captured by the LES equations and implies that additional modelling may not be required for sub-grid scale flame stretching. The results of [24] relate to cases for u'/s_L , the ratio of characteristic fluctuating velocity to laminar flame speed, up to about 11 and for Re_T , turbulence Reynolds number, up to about 110. They concluded that investigation should be extended to combustion at higher Re_T and to flows with shear, which are common in practical combustors.

In this contribution, we seek to extend the work of [24] by examining an experiment data set, rather than DNS, at high Re_T and including the effect of Lewis number. The preceding DNS analysis has been well controlled in every aspect, thereby opening the way for experimental observations to be explained with greater confidence: in addition, experimental data can be generated at substantially higher turbulent Reynolds number than is possible with DNS. There are differing opinions on the effect of increasing levels of turbulence (is there a higher impact of smaller scales of turbulence? Or change in the combustion regime in the Borghi-Peters diagram, for example?) so it is interesting to see if there is any consistency in the results. The experimental data used for this analysis are described in Section 2 and the bandpass filtering technique is discussed in Section 3. The results are presented and discussed in Section 4, and conclusions are summarised in the final section.

2. Experiments and Instrumentation

2.1. Burner

Three experiments were conducted on premixed, turbulent, V-flames stabilised on a 1.02 mm diameter stainless-steel wire, mounted 10 mm downstream of a square duct's exit plane: figure 1 shows elevation and isometric views. Sponfeldner ([26], [27]) describes the experiments in detail. The premixed reactant stream, fuel (methane or propane) and air, flowed through the square duct (600 x 62 x 62 mm) which contained a series of flow-conditioning elements and, lastly, a fractal 'square grid' (designated 'FG3' in [26]) to initiate a turbulent flow 100 mm upstream of the exit. Fractal grids ([28]) produce substantially larger turbulence intensities than regular grids and create vigorous turbulence near the flame, appropriate for the study of turbulence-flame interaction. A comprehensive description of the details of the evolution of the turbulence downstream of the grid can be found [29].

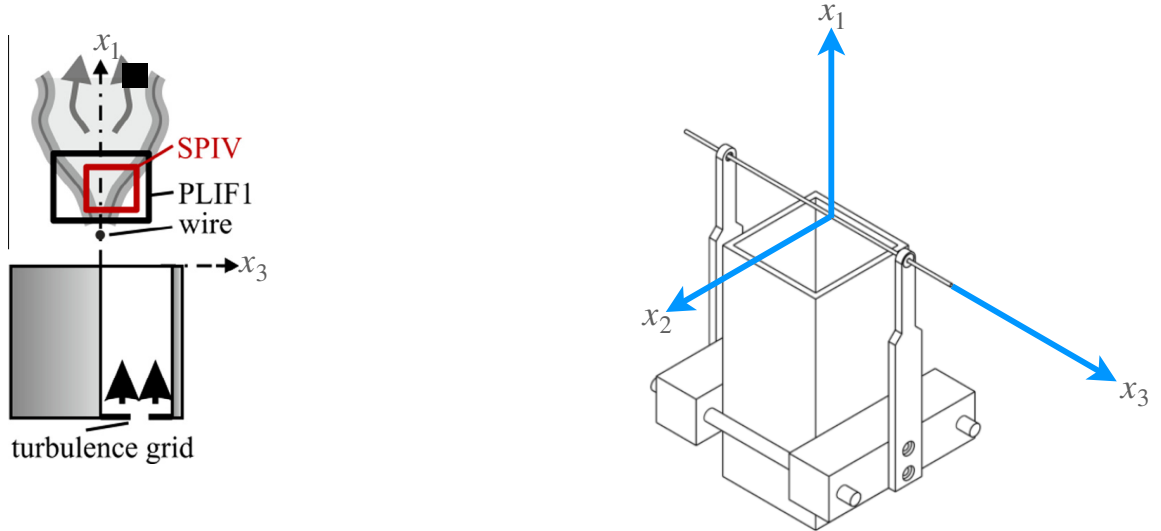


Figure 1: Schematic of the burner, wire flame holder and field of view of the PLIF (grey) and SPIV (red) instruments with the definition of the coordinate system (based on [27])

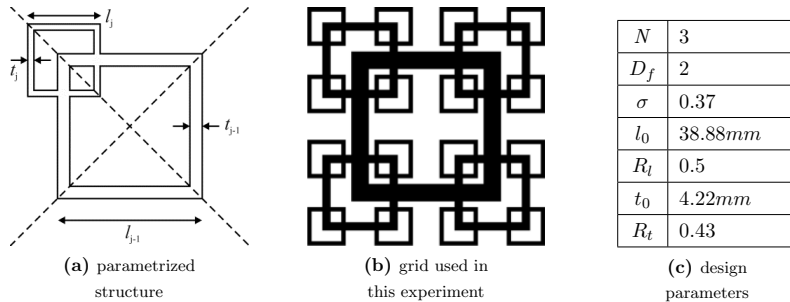


Figure 2: Fractal grid for generation of turbulence. D_f is the fractal dimension $D_f = -\log(4)/\log(R_l)$; N is the number of fractal iterations; $R_t = t_i/t_{i-1}$ and $R_l = l_i/l_{i-1}$ are the fractal iteration ratios for turbulence grid bar thickness, t , and length, l ; σ is the blockage ratio.

Measurements from a single-component hot-wire anemometer gave the axial mean and r.m.s.

fluctuating velocities, \bar{u}_1, u'_1 . Computation of the temporal autocorrelation of the x_1 (stream-wise) velocity gave the integral length scale, Λ , the Taylor microscale, λ , and the turbulent Reynolds number, Re_t , listed in Table 1. Equation 5 provides the means to calculate the Kolmogorov length scale, η , assuming homogeneous, isotropic turbulence (with ν being the kinematic viscosity):

$$\eta = \left(\frac{\nu^2 \lambda^2}{30 u_1'^2} \right)^{1/4} \quad (5)$$

Property	Value	Property	Value
\bar{u} (m/s)	5.5	u' (m/s)	0.75
Λ (mm)	9	Re_t	450
λ (mm)	3.6	η (mm)	0.12

Table 1: Isothermal turbulence properties at the flame stabilising wire and flame parameters ([26])

Flame	Fuel	ϕ	δ_{th} , mm	s_L , m/s	τ	Le	Da	Ka	Λ/δ_{th}	u'_1/s_L
1	CH ₄	0.8	0.55	0.25	5.8	1.01	5.45	0.83	16.4	3.0
2	CH ₄	0.9	0.48	0.33	6.3	1.01	8.25	0.49	18.8	2.3
3	C ₃ H ₈	0.9	0.45	0.36	6.4	1.83	9.6	0.42	20.0	2.1

Table 2: Properties of the three investigated flames. Details of calculation of δ_{th} , s_L , τ and Le in [27]

Table 2 summarises the properties of the three flames. Flame 1 was a methane-air flame with an equivalence ratio of 0.8. Flames 2 and 3 were selected to change both the laminar burning velocity, s_L and Lewis number, Le , variables which might have an effect of interest in this investigation. To do so, the equivalence ratio of Flame 2 was increased to $\phi = 0.9$ and for Flame 3 propane was used instead of methane. Flame 3 also had the largest laminar burning velocity while having the same heat release parameter, τ , as Flame 2. The magnitudes of the Damköhler Da and Karlovitz Ka numbers, together with values of the integral length scale Λ , the thermal flame thicknesses, δ_{th} , the characteristic turbulent velocity, u'_1 , and the laminar flame speeds s_L , placed the flames close to the boundary between the corrugated flamelet and thin reaction zone regimes, in the Borghi/Peters diagram figure 3. Flames 1, 2 and 3 are represented respectively by blocked orange circles: the flames studied in the work by Doan et al. [24] are represented by blocked blue circles. For convenience, table 2 summarises the values of Λ/δ_{th} and u'_1/s_L .

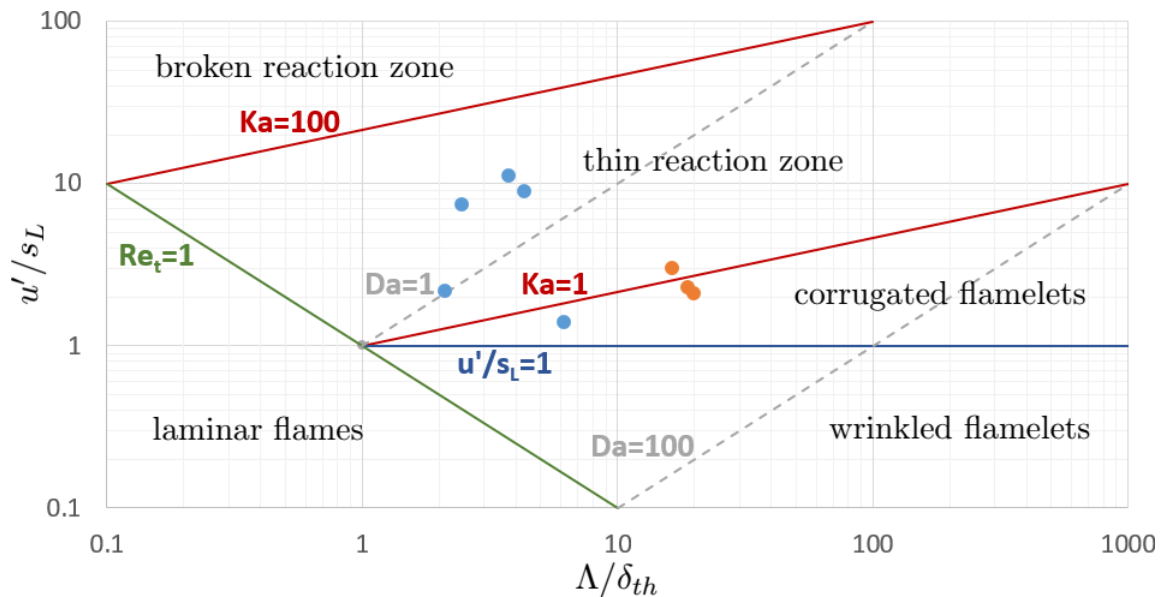


Figure 3: Borghi-Peters diagram

2.2. Stereoscopic particle image velocimetry

Stereoscopic particle image velocimetry (SPIV, details in [27]) measured the aerodynamic field in an x_1, x_2 plane. The principle features of the system are given in Table 3. Such measurements yielded four components only of the strain-rate tensor: this two-dimensional information of the strain-rate field is a tolerable estimate of the nine-component strain-rate tensor, e_{ij} , because the investigated flow field was also predominantly two-dimensional and close to homogeneous in the x_3 direction. This was because out-of-laser-sheet derivatives of velocity are small compared to the derivatives within the measurement plane. Velocity vectors were extracted from the particle images with vector resolution of 0.8 mm, that is to say at twice the vector spacing. The field of view was about 25mm by 22mm. Vector validation, and a 3 x 3 Gaussian smoothing filter, were applied to the vector fields for the subsequent analysis.

Table 3: SPIV parameters

Parameter	Value
Stereo-angle	90 deg.
Camera resolution HSS8	1024 x 1024 ($x_1 \times x_2$)
Camera resolution HSS6	1024 x 992 ($x_1 \times x_2$)
Field of view	25 mm x 21 mm
SPIV interrogation region	0.8 mm
Vector spacing	0.39 mm

2.3. Planar laser induced fluorescence

Planar laser-induced fluorescence imaging of the OH radical (OH-PLIF, details in [27]) was applied simultaneously in an imaging plane that was co-planar with that of the SPIV instrument to identify the reaction zone location of the flame in the SPIV measurement plane. OH-PLIF

1
2
3 images from flames in the thin flame regime permit the extraction of the flame front location by
4 the identification of the high gradient in the OH fluorescence signal between the unburnt and
5 burnt gases. The images were corrected for background noise, for inhomogeneities in the imaging
6 system sensitivity, and for non-uniform laser illumination. The corrected images were smoothed
7 with a Gaussian convolution filter (1.6mm kernel size) and a nonlinear diffusion filter (contrast
8 parameter 0.05, kernel 4 pixels, 25 iterations) to reduce noise and enhance flame contours.
9

10
11 In this work, an additional offset of the PLIF coordinates was applied until a satisfactory
12 alignment is achieved, by about 1.6mm (40 pixels), which was found to give the best result in
13 all the sampled frames.
14

15 16 17 **2.4. Data processing**

18
19 The experimental data provided the u_1 , u_2 and u_3 components of the velocity (respectively
20 along x_1 , x_2 and x_3 axis).
21

22 23 **2.4.1. Multiscale analysis method**

24
25 In the analysis to be performed in the next few sections, the multiscale analysis method used
26 is the bandpass filtering method presented in [25, 24] which allows us to reduce the effect of
27 eddies associated a particular ‘characteristic’ length scale L . A summary of the steps to execute
28 the method are described next. First, the original velocity field, \underline{u} , is Fourier transformed
29 and the Fourier coefficients, denoted $\hat{\underline{u}}$ where $\hat{\cdot}$ indicates the Fourier-transformed quantity,
30 are multiplied by a bandpass transfer function, $T_b(h) = \sqrt{8/L}h^2 \exp(h^2)$ with $h = kL/2$ where
31 $k = |\underline{k}|$ is the magnitude of the wavenumber. The spatial filter extends between about L and $4L$,
32 with a peak at $\sqrt{5}L$ and results in an instantaneous, spatially bandpass filtered velocity field,
33 denoted \underline{u}_b^L , appropriate to the chosen length scale L . Second, the resulting Fourier coefficients,
34 noted $\hat{\underline{u}}_b^L$, are then inverse Fourier-transformed to obtain the bandpass filtered velocity field, \underline{u}_b^L
35 which represents the effect of eddies which have a typical length scale L . Finally, using this
36 bandpass-filtered velocity field, further quantities of interest can then be computed related to
37 the specified length scale L , such as the vorticity field $\underline{\omega}^{L\omega} = \nabla \times \underline{u}_b^{L\omega}$, strain-rate e_{ij}^{Ls} , and
38 tangential strain rate a_T^{Ls} . However, given the planar nature of the measurements, the latter
39 quantity can be evaluated in a given x_1, x_2 plane only. Hence, the spatial derivatives in the x_3
40 direction remain unknown : $\frac{\partial u_1}{\partial x_3}, \frac{\partial u_2}{\partial x_3}, \frac{\partial u_3}{\partial x_3}$. This is also the case for $\frac{\partial c}{\partial x_3}$.
41
42
43
44
45

46 Several authors have discussed how to infer three-dimensional statistics from two-dimensional
47 data in the context of the flame surface density ([30]; [31]; [32], among others). [31] advised
48 linking the fluctuations in both transverse directions rather than relating the fluctuations in one
49 transverse-, and the downstream-, directions as initially proposed by[30]. [32] assumes the case
50 of isotropic scalar fields and turbulence and discusses the estimation of the tangential strain rate
51 in the flame surface density balance equation, arriving at a factor of 2 as the conversion factor
52 by which the two dimensional (measured) tangential strain should be multiplied to obtain the
53 three-dimensional result.
54
55
56

57 58 **2.5. Out-of-plane velocity derivatives approximation**

59
60 The approach to the problem of inferring three-dimensional statistics from two-dimensional data
61 adopted in this work was to analyse a DNS data set of a similar turbulent V-flame, to investigate
62
63
64
65

approximate values for the missing experimental components. The DNS data set, being fully three dimensional, had all velocity and c spatial derivatives available through finite differencing and thereby allows for a self-consistent analysis of velocity and scalar gradients. This approach allows us to deduce *qualitative* information which are consistent with many previous studies

The DNS data used here was generated by [33]: the simulation was fully compressible, three dimensional and the turbulence intensity $u'_1/s_L = 2$ is similar to that of the experimental flames presented in Table 2. The domain is a cube of side $12.77mm$, meshed with a 512^3 points uniform grid. The spatial step was $\approx 0.025mm$.

2.5.1. $\partial u_3/\partial x_3$ approximation

The adopted method was, with reference to the DNS data, to find two different approximations for reacting and non-reacting regions, to study the behaviour of $\frac{\partial u_3}{\partial x_3}$ relatively to the full ‘3D’ divergence of the flow and to the divergence of the flow based on the measured velocities restricted to the two dimensions (2D) of the laser sheet. It can be shown that [34]:

$$div(\underline{u}) = \frac{\tau}{1 + \tau c} \frac{Dc}{Dt} \quad (6)$$

where $\tau = \frac{T_b - T_u}{T_u}$ with T_b, T_u being the temperatures of the burnt products and unburnt reactants respectively. This equation, known as the dilatation equation, allows one to deduce the dilatation rate using the scalar field information at a given instant, which is often the case while post-processing saved DNS data, since $Dc/Dt = (\dot{\omega}_c + \nabla \cdot \rho \mathcal{D} \nabla c) / \rho$ (note that tomography with *high-speed* laser diagnostics will also allow the deduction of Dc/Dt directly and thus $\nabla \cdot \underline{u}$ can be estimated). From the definition of dilatation, we would have

$$\frac{\partial u_3}{\partial x_3} = div(\underline{u}) - \frac{\partial u_1}{\partial x_1} - \frac{\partial u_2}{\partial x_2} \quad (7)$$

and we introduce the quantity $div_{2D}(\underline{u})$

$$div_{2D}(\underline{u}) \equiv \frac{\partial u_1}{\partial x_1} + \frac{\partial u_2}{\partial x_2} \quad (8)$$

The separation of reacting from non-reacting regions was based on the spatial gradient of the reaction progress variable, $|\underline{grad} c| \leq 1mm^{-1}$ for non reacting regions and $|\underline{grad} c| > 1mm^{-1}$ for reacting regions. This results in the partition of the PIV window (figure 4). The sensitivity of the choice of the threshold level to discriminate between reactions and non-reacting regions has been investigated by halving, and doubling, the threshold gradient. We find that there is little influence.

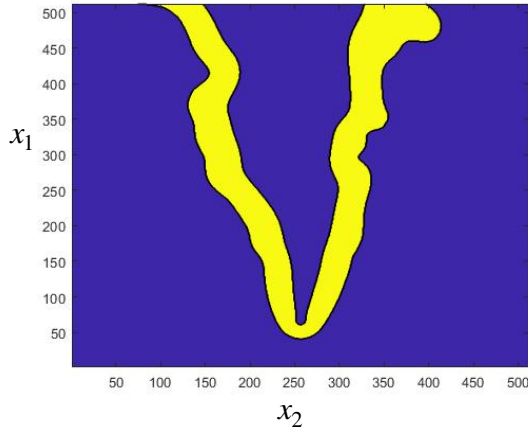


Figure 4: Partition of the PIV window: figure depicts the x_1, x_2 plane (numbers on ordinate and abscissa axes are in a.u.). Non-reacting regions in blue, reacting regions in yellow.

- *Non reacting regions*

Figures 5 and 7 show that the 3D divergence is very close to zero for a large majority of grid points (the error being associated with the method of separating the reacting from the non-reacting regions of the flow). This is confirmed by figure 9 which shows that the zero divergence assumption is a good approximation : $\frac{\partial u_3}{\partial x_3} \approx -\frac{\partial u_1}{\partial x_1} - \frac{\partial u_2}{\partial x_2}$. This assumption was used when processing experimental data for non-reacting regions.

- *Reacting regions*

Figures 6 and 8 show that in combustion, as expected, the divergence increases considerably towards positive values and figure 10 confirms that the no divergence assumption is invalid. However, importantly, Figure 6 shows that the measured $div_{2D}(\underline{u})$ is a tolerable approximation to $div_{3D}(\underline{u})$. Hence, the contribution of $\frac{\partial u_3}{\partial x_3}$ to $div_{2D}(\underline{u})$ is here neglected in reacting regions $\frac{\partial u_3}{\partial x_3} = 0$ was the assumption adopted for reacting regions.

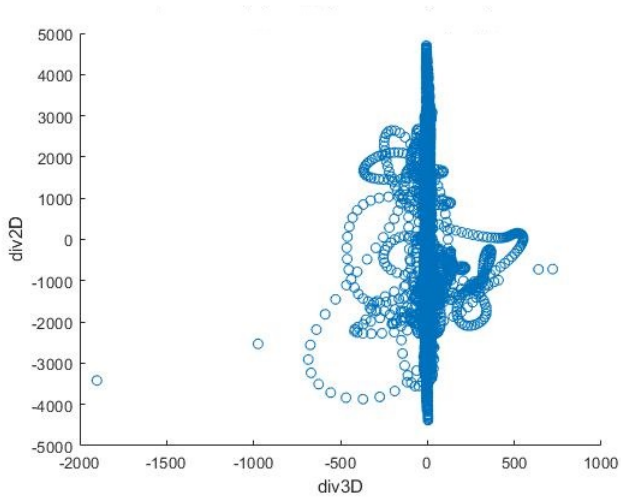


Figure 5: div_{2D} against div_{3D} in non reacting regions

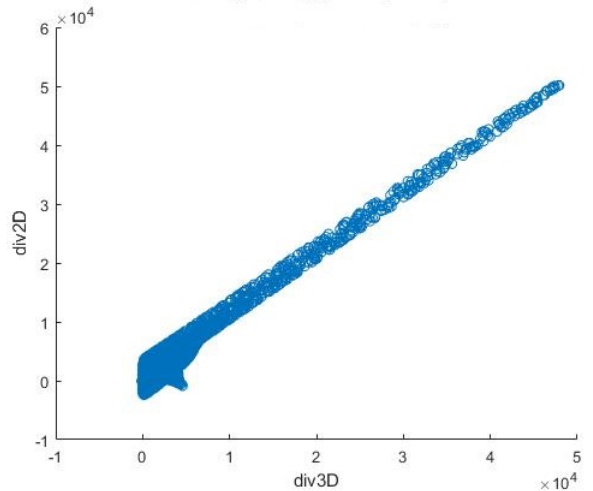


Figure 6: div_{2D} against div_{3D} in reacting regions

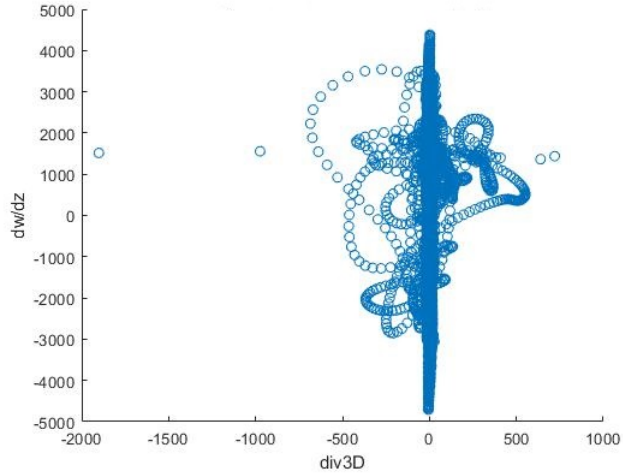


Figure 7: $\frac{\partial u_3}{\partial x_3}$ against div_{3D} in non reacting regions

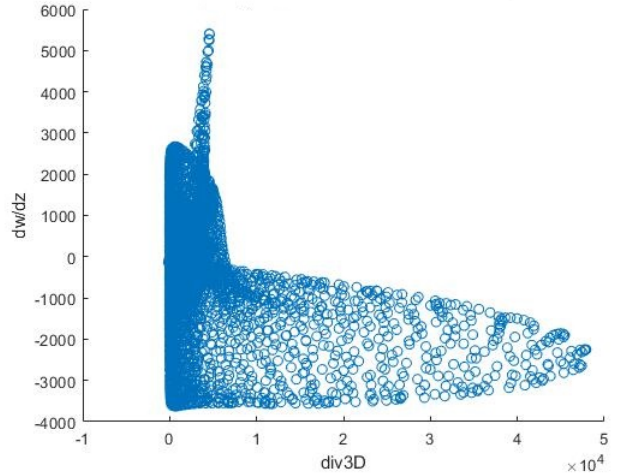


Figure 8: $\frac{\partial u_3}{\partial x_3}$ against div_{3D} in reacting regions

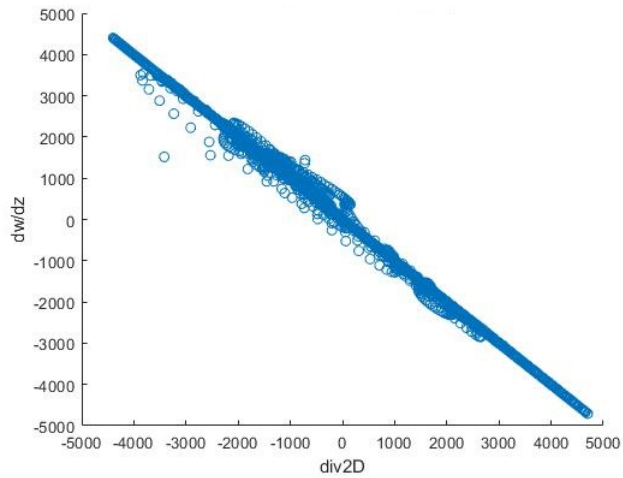


Figure 9: $\frac{\partial u_3}{\partial x_3}$ against div_{2D} in non reacting regions

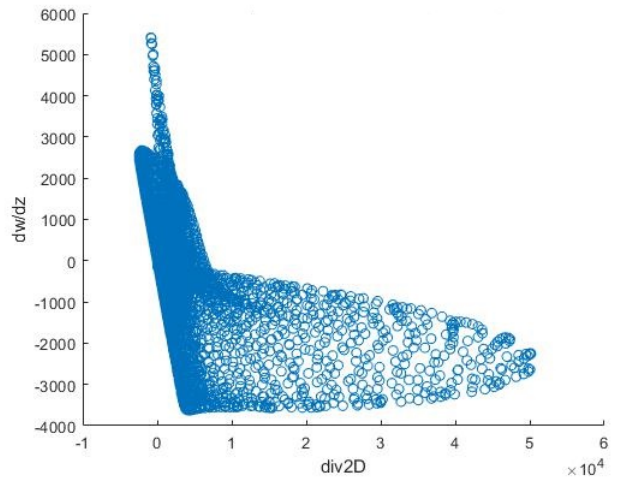


Figure 10: $\frac{\partial u_3}{\partial x_3}$ against div_{2D} in reacting regions

2.5.2. $\partial u_1/\partial x_3$ and $\partial u_2/\partial x_3$ approximation

The method for these two terms, once again in relation to the DNS data, is to use random distributions, on the basis that we expect - in this flow which is a close approximation to being two-dimensional in the mean in the x_1, x_2 plane - neither $\partial u_1/\partial x_3$ nor $\partial u_2/\partial x_3$ to be correlated with other terms in the rate of strain tensor. This in turn is owing to there being, in the mean, no shear stress in the x_1, x_3 plane. This method comes down to using two randomly generated matrices a and b such as

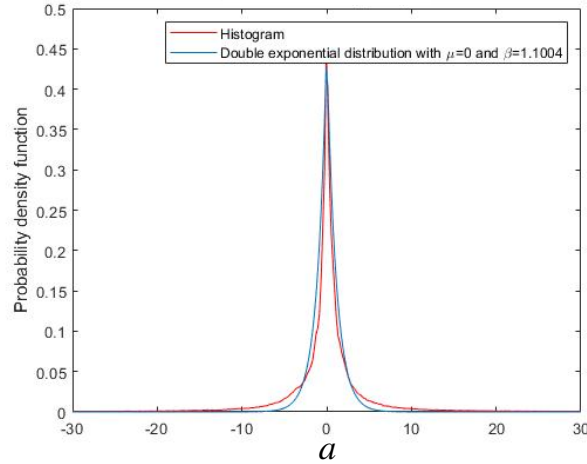
$$\frac{\partial u_1}{\partial x_3} = a \frac{\partial u_1}{\partial x_1} \quad (9)$$

$$\frac{\partial u_2}{\partial x_3} = b \frac{\partial u_2}{\partial x_2} \quad (10)$$

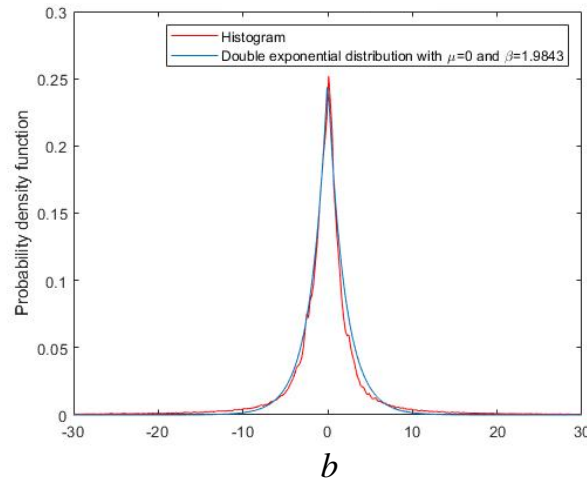
1
2
3 The DNS data set was used to find distributions for a and b components. A double exponential
4 distribution is chosen, defined by its Probability Density Function (PDF) :

$$pdf(v) = \frac{1}{2\beta} \exp\left(-\frac{|v - \mu|}{\beta}\right) \quad (11)$$

10 where v is either a or b , as appropriate. The best-fit parameters determined for both matrices
11 were zero mean velocity, $\mu_a = \mu_b = 0$, and $\beta_a = 1$ and $\beta_b = 1.9$. The degree of fit is shown in
12 Figures 11 and 12. The error that we incur with this practice is expected to be small because
13 the experimental frame is statistically two dimensional. It is difficult to quantify the resulting
14 error without full data.
15
16
17



18
19
20
21
22
23
24
25
26
27
28
29
30
31
32
33
34
35 Figure 11: Double exponential fitting (blue) of the DNS data (red) for values of the a matrix



36
37
38
39
40
41
42
43
44
45
46
47
48
49
50
51
52
53
54
55
56
57 Figure 12: Double exponential fitting (blue) of the DNS data (red) for values of the b matrix

2.6. Reaction progress variable gradient approximation, $\partial c/\partial x_3$

No method for recovering $\frac{\partial c}{\partial x_3}$ has been found. Instead, our aim is to show that its contribution to the tangential strain rate is small, which is to say that n_3 is negligible. This hypothesis may be countenanced by the fact that the x_3 direction is close to spatially homogenous on average, hence there must be little variation along it. First, we define the reactive contribution a_T^r to the tangential strain rate :

$$a_T^r = n_i n_j e_{ij} \quad (12)$$

The terms of a_T^r involving n_3 are compared to a_T^r . Those terms are $n_1 n_3 e_{13}$, $n_2 n_3 e_{23}$ and $n_3 n_3 e_{33}$. It is found that these are not negligible in a substantial part of the window: Figure 13 shows this for one term, $n_3 n_3 e_{33}$ normalised by $n_3 n_3 e_{33} + a_T^r$, and a similar result is found for the other two.

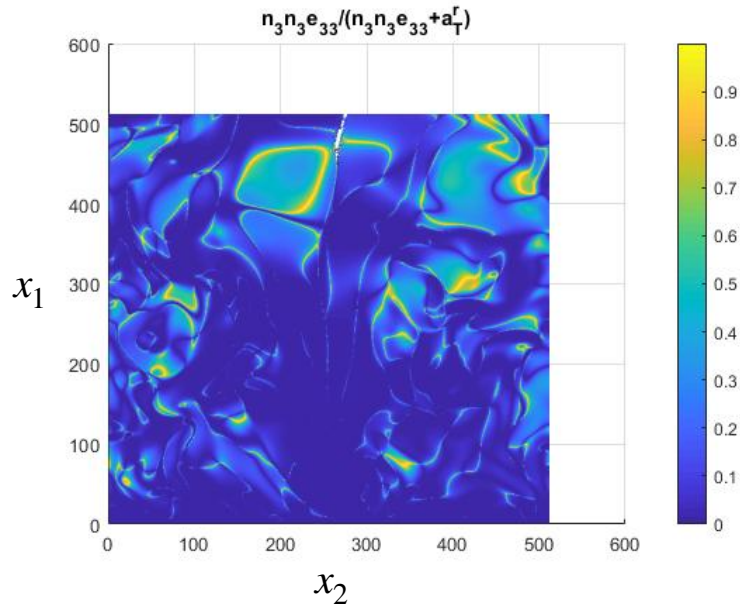


Figure 13: Contribution of $n_3 n_3 e_{33}$ to the reactive part of the tangential strain rate, normalised by $n_3 n_3 e_{33} + a_T^r$. (numbers on ordinate and abscissa axes are in a.u.).

We perform the multiscale analysis with the assumption of $n_3 = 0$, which aims to highlight whether there exists a peak contribution at a certain length scale, below which the contribution to the flame stretch would plummet. The presented method is taken from the work of Doan *et al.* [24] and the quantity of interest is the surface averaged strain rate ψ for a given bandpass filtered scale L_s :

$$\psi(L_s^+) = \langle |\nabla c| a_T^{L_s^+} \rangle / \langle |\nabla c| \rangle \quad (13)$$

with $L_s^+ = L_s/\delta_{th}$ being the normalised bandpass filtered scale and $a_T^{L_s} = (\delta_{ij} - n_i n_j) e_{ij}^{L_s}$ the bandpass filtered tangential strain rate. The divergence of c is taken as a proxy for the flame surface density by which one weights the quantity of interest. So a large divergence of c means

locally large surface. The definition was originally for a thin flame but can be generalised to a thick flame [5]. The fractional contribution of each scale is $\widehat{\psi}(L_s^+) = \psi(L_s^+)/\psi_{int}$, where $\psi_{int} = \int_0^\infty \psi dL_s^+$.

In Figure 14 $\widehat{\psi}$ is plotted against the range of filtered scales for two different time frames from the DNS set, using both the exact n_3 and the assumption of $n_3 = 0$. We find that the location of the peaks, although not the magnitude of the peaks, is almost independent of the previous assumption.

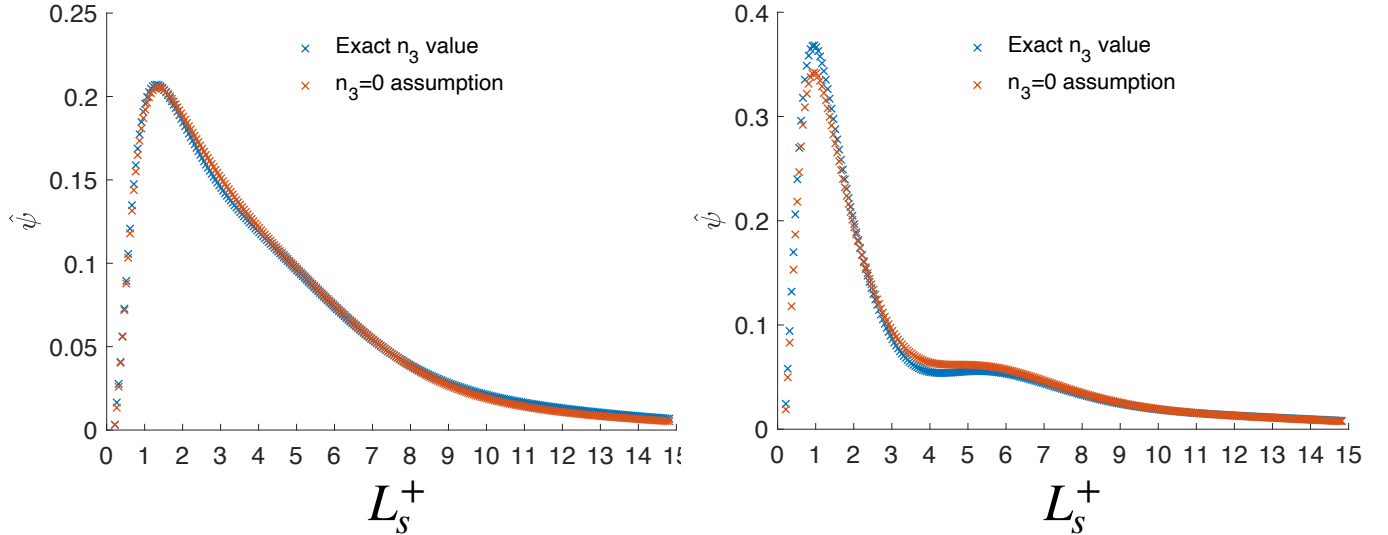


Figure 14: Surface averaged tangential strain rate, $\widehat{\psi}$, from eddies characterised by bandpass filtering scale scale L_s^+ , normalised by total contribution for $u'/S_L = 2$. The figures are generated from two different time frames from the DNS set.

The $\frac{\partial c}{\partial x_3}$ term is involved in the analysis of the flame stretch only. Hence, as for the experimental data, the multiscale analysis will be conducted under the same assumption of $n_3 = 0$ below.

3. Experimental Results

3.1. Influence of combustion on vortex stretching

The question to be addressed in this sub-heading is whether combustion modifies the vortex stretching mechanism, by reference to non-reacting flow, whereby eddies of smaller size are produced by the stretching and subsequent breaking of larger eddies. Here, this is investigated in terms of the alignment between the vorticity vector of a filtered field, $\underline{\omega}^{L_\omega}$, and principal component of a filtered strain rate tensor, $e_{ij}^{L_s}$. Note that L_ω and L_s are independent variables and not necessarily equal. The most extensional, the most compressive, and intermediate principal components are denoted by α^{L_s} , γ^{L_s} and β^{L_s} respectively and the degree of alignment is given by the cosine of the angles, θ_i , between the vorticity vector and the principal components ($i = \alpha, \beta, \gamma$). To produce enstrophy through stretching, the vorticity has to align with α^{L_s} or

1
2
3 positive part of β^{L_s} . In this work, we concentrate on the most extensional principal component.
4 The probability function, discretised into 64 bins of width $1/64 \approx 0.015$, of $|\cos \theta_\alpha|$ for bandpass
5 filtered fields of premixed flame with $u'/s_l = 3.0$, is shown in Figure 15 for $L_\omega = 4 \delta_{th}$ and $2\delta_{th} \leq$
6 $L_s \leq 16\delta_{th}$. The presented results are for the non reacting regions of the flow only, *i.e.* where
7 $|\underline{grad} c| < 1mm^{-1}$, although we include regions both upstream and downstream of the flame
8 front. All figures below are the result of averaging well over 2000 images. We perform the
9 analysis for the whole domain (which contains regions both close to the flame and further from
10 the flame effects) to have a general view on what is happening. We anticipate the results below
11 by stating that we observed similar behaviour to that for non-reacting turbulence so there was
12 no strong effect of the flame on this vortex stretching mechanism (as could have been possible,
13 for example, in the downstream region after the flame dissipated some turbulence).
14
15
16

17 The uncertainties in the results below, based on estimates of the vorticity and rate of strain,
18 stem from uncertainty in the measurement of velocity by a PIV and the corresponding error
19 in the estimation of velocity gradients due to the finite spatial resolution of the PIV and the
20 implied spatial averaging (in these experiments, we expect errors from out-of-plane convection
21 and gradients on the results to be small in this flow because it is two dimensional in the
22 mean). [35] quantified these sources by reference to DNS calculations in homogeneous isotropic
23 turbulence. They advise a spatial resolution (to minimise loss of fine scale information) of the
24 order of $2 - 3\eta$, as used here, to resolve fine scale features and they report levels of gradient
25 uncertainty at around 20 percent. In an experiment closer to that reported in this work, [17]
26 and [18] also indicate that a spatial resolution of 3η results in estimates of gradients that do not
27 suffer from excessive smoothing. [17] report that for ω_i and e_{ij} , the maximum RMS error is be
28 expected as less than 7 per cent. The uncertainty in the estimation of $|\cos \theta_i|$ is related to those
29 in ω_i and e_{ij} and we thus estimate these quantities to be around 15 percent. The additional
30 errors that arise during the computation of the strain-rate on the flame, a_T , they estimate as
31 less than 10 per cent.
32
33
34
35
36

37 Figure 15 shows that, for the most extensional principal component, α , the results are quali-
38 tatively consistent with [24] in that indeed vorticity is more likely to be aligned with the most
39 extensive α strain direction, at all investigated scales of L_s , from 2 to 16 δ_{th} , although here
40 there is also evidence of prevalence at $|\cos \theta_\alpha| = 0$. However, we are unable to confirm their
41 observation that such preferential alignment disappears abruptly below $L_s = 3 \delta_{th}$ because we
42 present results for a vortical structure of $L_\omega = 4\delta_{th}$ only while [24] were able to consider $L_\omega = \delta_{th}$.
43 This is a limitation of the experimental apparatus where we cannot have as high a resolution
44 as in DNS and we therefore cannot assess the impact of these smaller scales of turbulence.
45 However, from past studies from DNS [24], we see that the most important scales of turbulence
46 are generally larger than the flame thermal thickness. So, the analysis that we can obtain from
47 these data is still meaningful.
48
49
50
51
52
53
54
55
56
57
58
59
60
61
62
63
64
65

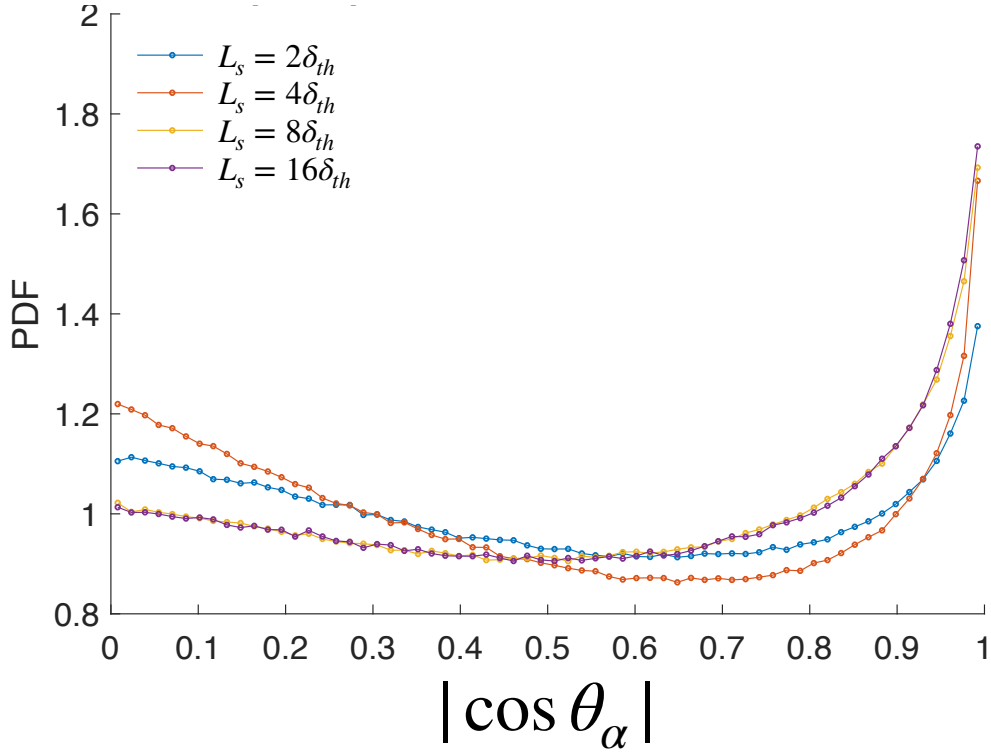


Figure 15: Probability of alignment ($|\cos \theta_\alpha|$) between vorticity at scale $L_\omega = 2\delta_{th}$ and principal strain rate α with scale L_s ($L_s = 2\delta_{th}, 4\delta_{th}, 8\delta_{th}, 16\delta_{th}$) as parameter with $u'/s_L = 3.0$ for flame 1

Figure 16, for flame 1 in Table 2, quantifies which eddy length scales L_s impart the most stretch on vortical structures of scale $L_\omega = 2\delta_{th}, 4\delta_{th}$ and $6\delta_{th}$ by presenting the probability, P , for $63/64 \leq |\cos \theta_\alpha| \leq 1$ with the magnitude of L_ω as parameter. The figure shows that there is, consistently, a broad peak between 2 and 4 times the considered value of $L_\omega \delta_{th}$ (to avoid ambiguity, this means that the peak for $L_\omega = 6\delta_{th}$, which is at about $2.6L_\omega$, corresponds to $L_s \approx 2.6 \cdot 6 \cdot \delta_{th}$) which accords with the expectation from the non-reacting work of [25]. Of greater direct relevance is that there is also qualitative agreement with the findings of [24] in premixed flames, although they were able to resolve down to $L_\omega = \delta_{th}$ which we are not able to with this data set.

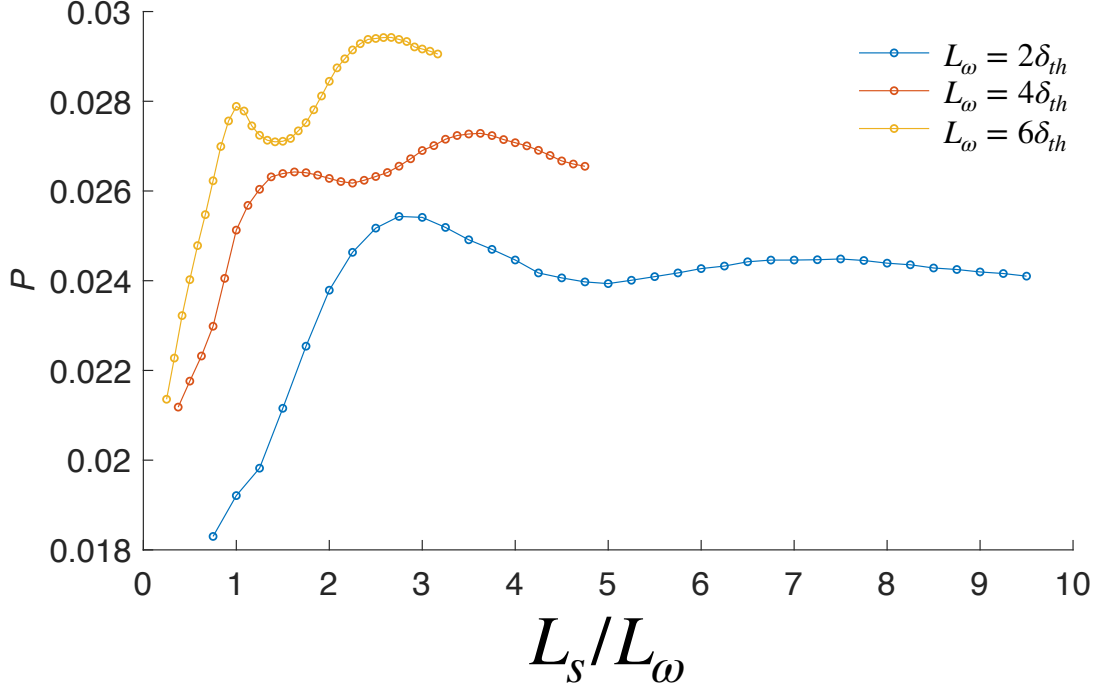


Figure 16: Probability of alignment ($63/64 \leq |\cos \theta_\alpha| \leq 1$) between vorticity at scale L_ω and principal strain rate α at scale L_s with the magnitude of L_ω ($L_\omega = 2\delta_{th}, 4\delta_{th}, 6\delta_{th}$) as parameter for flame 1.

3.2. Multiscale analysis of tangential strain rate

We estimate, as above, the normalised surface averaged tangential strain rate, $\hat{\psi}$, from eddies of normalised bandpass filtered scale L_s^+

$$\hat{\psi}(L_s^+) = \psi(L_s^+) / \psi_{int} \quad (14)$$

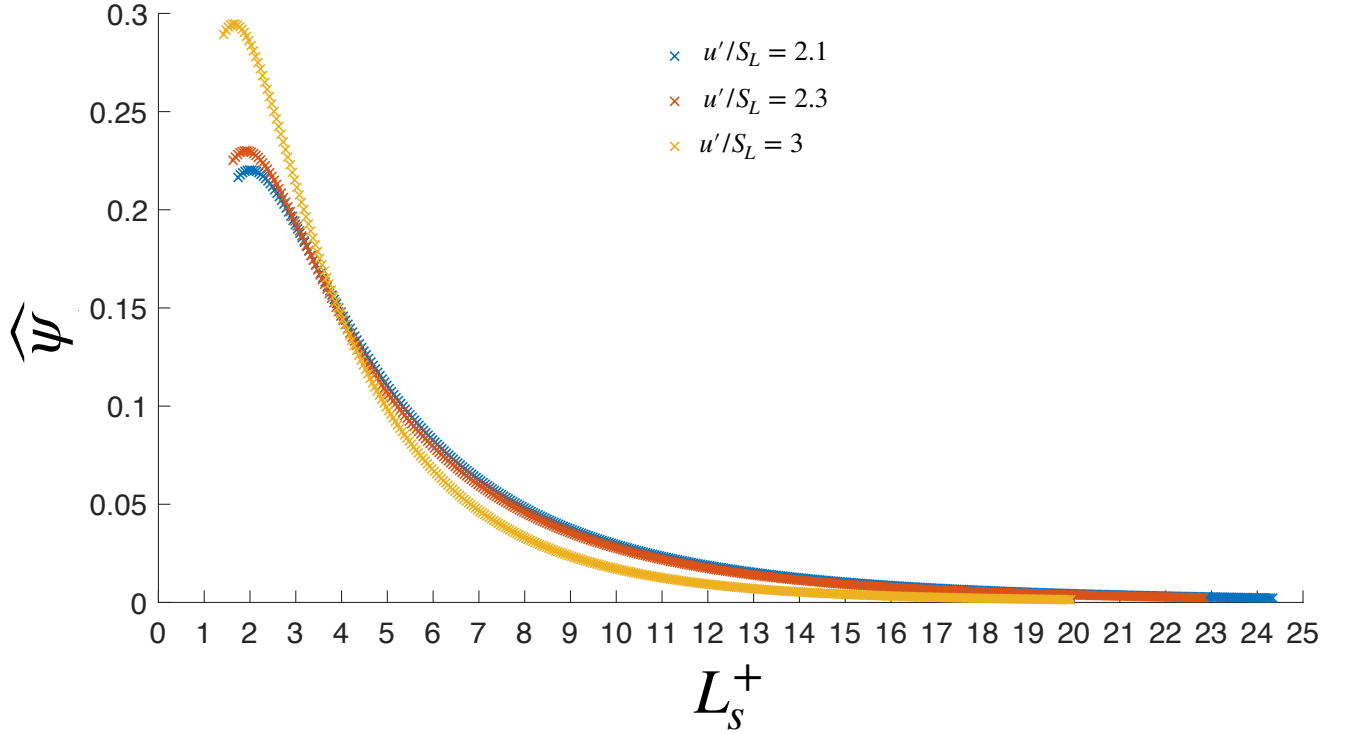


Figure 17: Surface averaged tangential strain rate, $\psi(L_s^+)$, from eddies of scale L_s^+ , normalised by total contribution, ψ_{int} : $\hat{\psi} = \psi(L_s^+)/\psi_{int}$. Flames 1, 2, 3 averaged over 2816 frames.

where the quantities involved have been defined for equation 13. Figure 17 shows the variation of the fractional contribution $\hat{\psi} = \psi/\psi_{int}$ with L_s^+ for flames 1, 2 and 3. The resolution of our data does not allow the determination of the location of the maximum contribution with confidence, other than to say that it is consistently below $L_s^+ \approx 2$ in our measurements. Note that the slight evidence of the maximum in the figure is not due to curve fitting, but due to measurement: indeed, more convincing maxima are to be found in individual frames. Also, the differences between the three flames in terms of Lewis number, which is arguably the main distinguishing parameter between these, and to a lesser extent the laminar burning velocity, does not result in any noticeable change in the shape of the dependence. It is worth noting that the length scale of $L_s^+ \simeq 2$ is similar to the inner cut-off scale estimates based on fractal analysis of flame surface density [36, 37, 38, 39, 40, 41, 42, 43, 44, 45, 46, 47, 48] and scalar dissipation rate closures [49].

For flames with u'/s_L comparable to those here, [24] found peaks between $5 \leq L_s^+ \leq 10$ which are higher values than in our experiments: however, for flames with higher turbulence intensity, they found that the peak value is shifted towards values of L_s^+ of about 2 to 3, which is closer to our findings. The differences may be related to the much higher turbulence Reynolds number of the experiments. Furthermore, the rapid decrease in contributions from eddies of sizes larger than that associated with the peak in the experiments has some parallel with the higher turbulence intensity flames of [24] up to $L_s^+ \approx 6$. Nevertheless, the results presented here do not have the resolution down to the smallest values of L_s^+ and therefore we cannot reliably estimate the relative contribution of eddies smaller than, say, $2\delta_{th}$ on the total tangential strain rate. A crude estimate is that it is of the order of 1/3, which is larger than the value of 10 per cent found by [24]. In summary, the current experiments suggest that the range of eddies which

1
2
3 have a substantial effect on flame straining is comparable to the range found by Doan, namely
4 $3 \leq L_s^+ \leq 17$.

5
6 Estimates for the smallest length scales include that of [20], L_R

$$(L_R/\delta_{th}) = (u'/s_L)^{-3/4} (\Lambda/\delta_{th})^{1/4} \quad (15)$$

7
8
9
10
11
12 Table 4: L_R [20] and Gibson cutoff scales

Flame	L_R/δ_{th}	L_G/δ_{th}
1	1.8	3.3
2	2.2	8.7
3	0.9	12.1

13
14
15 and the Gibson scale $L_G = s_L^3/\epsilon$. Values for these length scales, normalised by δ_{th} , are given
16 in Table 4 (where we estimate $\epsilon = 15\nu u'^2/\lambda^2$). These values are higher than the corresponding
17 values in [24], once again presumably because of the higher turbulent Reynolds number in the
18 experiments but, particularly given the uncertainty in the estimate of ϵ , the range of eddies
19 having weak influence in straining flame needs further examination.

20
21 The broader conclusion of [24] stands, however, in that it is turbulent structures larger than
22 about $2\delta_{th}$ which have substantial effect and thus it may be unnecessary to resolve smaller scales.
23 Here it is recalled that the bandpass filter has a sharper roll-off at scales smaller than the ‘centre’
24 value than at larger scales. Thus the results here are, as noted by [24], conservative estimates
25 and the practical implication is that, in large eddy simulations (LES), the effort required to
26 resolve scales as small as δ_{th} may be unnecessary. This is a tentative conclusion which certainly
27 deserves further experimental study over a wider range of parameter space in the Borghi-Peters
28 diagram, with instrumentation that permits resolution of $L_\omega = \delta_{th}$ and is able to resolve the
29 full rate of strain tensor.

30 31 32 33 34 35 36 37 38 39 40 41 42 43 44 45 46 47 48 49 50 51 52 53 54 55 56 57 58 59 60 61 62 63 64 65

44 We have applied bandpass multiscale analysis to three sets of experimental measurements of
45 premixed, turbulent, V-flames straddling the border between corrugated flamelets and thin
46 reaction zone in the Borghi-Peters diagram. The turbulent Reynolds number investigated here
47 is a factor of about four larger than that examined previously using DNS, while the ratio of
48 characteristic turbulent velocity to laminar flame speed, u'/s_L , is between 2 and 3 while the DNS
49 studies extended this to about 11. For each flame there is a comprehensive data set in one plane
50 only. Approximations for the missing out-of-plane derivatives have been constructed, aided by
51 the flow being close to two - dimensional on average, and by recourse to comparisons with a
52 DNS calculation of a similar flow. For $\partial u_3/\partial x_3$ we have used the approximation $-\partial u_1/\partial x_1 -$
53 $\partial u_2/\partial x_2$ in non-reacting regions, and $\partial u_3/\partial x_3 = 0$ where reaction takes place. For the out-of-
54 measurement-plane gradients of velocity, we have used exponential distributions curve-fitted to
55 the results from the DNS calculation for the probability functions of $\partial u_1/\partial x_3$ and $\partial u_2/\partial x_3$. For
56 the calculation of the reactive strain rate, we have used the approximation that $n_3 = 0$, once
57 again verifying the effect of doing so by recourse to the DNS data and finding that the effect is
58 negligible.

1
2
3 This work quantifies two aspects of turbulence-flame interaction. The first aspect is that of
4 the flame interaction of eddies of size L_s on the turbulence as found by the statistics of the
5 alignment of vorticity with strain rate. We find that vortical eddies with scale about $L_\omega = 2\delta_{th}$
6 are stretched by L_s structures which are larger than about $2 L_\omega$, with this factor broadly true
7 also for vortical eddies of scales $L_\omega = 4\delta_{th}$ and $L_\omega = 6\delta_{th}$. Within the limitations of the data
8 set, these findings are comparable to those of [24] in reacting and [25] in non-reacting flows,
9 although these authors were able to investigate resolutions down to $L_\omega = \delta_{th}$. [24] concluded
10 that the premixed flame had negligible influence on the vortex stretching mechanism and our
11 results here are consistent with this finding.
12
13
14

15 The second aspect of turbulence-flame interaction examined is that of flame surface averaged
16 tangential strain rate imparted by eddies. Eddies with length scales L_s smaller than $2\delta_{th}$ have
17 the strongest individual contribution but may nevertheless contribute only about 1/3 of the
18 total tangential strain rate. This is larger than the 10 % that has been reported by [24] based
19 on analysis of DNS predictions of premixed flames at turbulent Reynolds numbers up to 110.
20 Eddies with length scale L_s larger than about $20\delta_{th}$ contribute a negligible amount to the total
21 tangential strain rate. The latter conclusion is also in accordance with that of [24].
22
23
24

25 In the context of large eddy simulations (LES) of premixed combustion, these results are pre-
26 liminary experimental evidence into the suggestion [24] that resolving turbulence scales down
27 to a few multiples of δ_{th} might be adequate to capture much of the flame straining caused
28 by turbulence. Further experimentation is required, with instruments which can resolve scales
29 close to the flame thickness, permit estimation of the full rate of strain tensor without the
30 approximations used here; and for a broader area in the Borghi-Peters diagram. The aim of
31 further work is to establish the range of conditions flames that can be calculated adequately
32 by LES equations without additional modelling to describe sub-grid scale flame stretching. We
33 have found no evidence that the Lewis number up to about 1.8 has an observable effect, but
34 this may reflect the inability of the current instruments to resolve vortical structures down to
35 $L_\omega = \delta_{th}$. This is a topical question in view of the possible widespread adoption of hydrogen,
36 and its related vector fuels, in future combustion systems.
37
38
39
40
41

42 Acknowledgements

43

44 We thank Dr Tom Dunstan for the use of the DNS data that he calculated. Dr Antonis Sergis
45 helped us with the management of the archiving of the large experimental data set.
46
47
48
49
50
51
52
53
54
55
56
57
58
59
60
61
62
63
64
65

References

- [1] K. Bray, The interaction between turbulence and combustion, *Symp. (int.) Combust.* 17 (1) (1979) 223–233.
- [2] K. Bray, The challenge of turbulent combustion, *Symp. (int.) Combust.* 26 (1) (1996) 1–26.
- [3] S. M. Candel, T. J. Poinso, Flame Stretch and the Balance Equation for the Flame Area, *Combust. Sci. Technol.* 70 (1-3) (1990) 1–15.
- [4] N. Peters, *Turbulent Combustion*, Cambridge University Press, Cambridge, 2000.
- [5] D. Veynante, L. Vervisch, Turbulent combustion modeling, *Prog. Energy Combust. Sci.* (2002) 74.
- [6] E. R. Hawkes, R. S. Cant, Implications of a flame surface density approach to large eddy simulation of premixed turbulent combustion, *Combust. Flame* 126 (01) (2001) 1617–1629.
- [7] N. Chakraborty, M. Klein, R. S. Cant, Stretch rate effects on displacement speed in turbulent premixed flame kernels in the thin reaction zones regime, *Proc. Combust. Inst.* 31 (1) (2007) 1385–1392.
- [8] S. Ruan, N. Swaminathan, Y. Mizobuchi, Investigation of Flame Stretch in Turbulent Lifted Jet Flame, *Combust. Sci. Technol.* 186 (3) (2014) 243–272.
- [9] C. Dopazo, L. Cifuentes, J. Martin, C. Jiménez, Strain rates normal to approaching isoscalar surfaces in a turbulent premixed flame, *Combust. Flame* 162 (5) (2015) 1729–1736.
- [10] O. Colin, F. Ducros, D. Veynante, T. Poinso, A thickened flame model for large eddy simulations of turbulent premixed combustion, *Phys. Fluids* 12 (7) (2000) 1843–1863.
- [11] F. Charlette, C. Meneveau, D. Veynante, A power-law flame wrinkling model for LES of premixed turbulent combustion Part I: Non-Dynamic formulation and Initial Test, *Combust. Flame* 131 (02) (2002) 159–180.
- [12] H. Pitsch, Large-Eddy Simulation of Turbulent Combustion, *Annu. Rev. Fluid Mech.* 38 (1) (2006) 453–482.
- [13] H. Kolla, N. Swaminathan, Strained flamelets for turbulent premixed flames, I: Formulation and planar flame results, *Combust. Flame* 157 (5) (2010) 943–954.
- [14] C. Meneveau, T. Poinso, Stretching and quenching of flamelets in premixed turbulent combustion, *Combust. Flame* 86 (4) (1991) 311–332.
- [15] S. Bougrine, S. Richard, O. Colin, D. Veynante, Fuel Composition Effects on Flame Stretch in Turbulent Premixed Combustion: Numerical Analysis of Flame-Vortex Interaction and Formulation of a New Efficiency Function, *Flow, Turbul. Combust.* 93 (2) (2014) 259–281.
- [16] F. Thiesset, G. Maurice, F. Halter, N. Mazellier, C. Chauveau, Flame-vortex interaction : effect of residence time and formulation of a new efficiency function, *Proc. Combust. Inst.* 000 (2015) 1–9.

- 1
2
3 [17] A. M. Steinberg, J. F. Driscoll, Straining and wrinkling processes during turbu-
4 lence-premixed flame interaction measured using temporally-resolved diagnostics, *Com-
5 bust. Flame* 156 (12) (2009) 2285–2306.
6
7 [18] A. M. Steinberg, J. F. Driscoll, Stretch-rate relationships for turbulent premixed combus-
8 tion LES subgrid models measured using temporally resolved diagnostics, *Combust. Flame*
9 157 (7) (2010) 1422–1435.
10
11 [19] T. Poinso, D. Veynante, S. M. Candel, Quenching processes and premixed turbulent com-
12 bustion diagrams, *J. Fluid Mech.* 228 (1991) 561–606.
13
14 [20] W. L. Roberts, J. F. Driscoll, M. C. Drake, L. P. Goss, Images of the quenching of a flame
15 by a vortex—To quantify regimes of turbulent combustion, *Combust. Flame* 94 (1) (1993)
16 58–69.
17
18 [21] A. N. Lipatnikov, S. Nishiki, T. Hasegawa, A direct numerical simulation study of vorticity
19 transformation in weakly turbulent premixed flames, *Phys. Fluids* 26 (10) (2014) 105104.
20
21 [22] Y. Nada, M. Tanahashi, T. Miyauchi, Effect of turbulence characteristics on local flame
22 structure of H₂-air premixed flames, *J. Turbul.* 5 (2004) 37–41.
23
24 [23] B. Yenerdag, N. Fukushima, M. Shimura, M. Tanahashi, T. Miyauchi, Turbulence-flame
25 interaction and fractal characteristics of H₂-air premixed flame under pressure rising con-
26 dition, *Proc. Combust. Inst.* 35 (2) (2015) 1277–1285.
27
28 [24] N. Doan, N. Swaminathan, N. Chakraborty, Multiscale analysis of turbulence-flame inter-
29 action in premixed flames, *Proc. Combust. Inst.* 36 (2) (2017) 1929–1935.
30
31 [25] T. Leung, N. Swaminathan, P. A. Davidson, Geometry and interaction of structures in
32 homogeneous isotropic turbulence, *J. Fluid Mech.* 710 (2012) 453–481.
33
34 [26] T. Sponfeldner, I. Boxx, F. Beyrau, Y. Hardalupas, W. Meier, A. M. K. P. Taylor, On the
35 alignment of fluid-dynamic principal strain-rates with the 3D flamelet-normal in a premixed
36 turbulent V-flame, *Proc. Combust. Inst.* 35 (2) (2015) 1269–1276. doi:10.1016/j.proci.
37 2014.06.082.
38
39 [27] T. Sponfeldner, The effect of fractal grid generated turbulence on the structure of premixed
40 flames, Ph.D. thesis, Imperial College London, London U.K. (2014).
41
42 [28] D. Hurst, J. C. Vassilicos, Scalings and decay of fractal-generated turbulence, *Phys. Fluids*
43 19 (3) (2007) 035103, publisher: American Institute of Physics.
44
45 [29] N. Soulopoulos, J. Kerl, T. Sponfeldner, F. Beyrau, Y. Hardalupas, A. M. K. P. Taylor,
46 J. C. Vassilicos, Turbulent premixed flames on fractal-grid-generated turbulence, *Fluid
47 Dyn. Res.* 45 (6) (2013) 061404.
48
49 [30] F. Halter, C. Chauveau, I. Gokalp, D. Veynante, Analysis of flame surface density mea-
50 surements in turbulent premixed combustion, *Combust. Flame* 156 (3) (2009) 657–664.
51
52 [31] D. Veynante, G. Lodato, P. Domingo, L. Vervisch, E. R. Hawkes, Estimation of three-
53 dimensional flame surface densities from planar images in turbulent premixed combustion.,
54 *Exp. Fluids* 49 (1) (2010) 267–278.
55
56
57
58
59
60
61
62
63
64
65

- 1
2
3 [32] E. R. Hawkes, R. Sankaran, J. H. Chen, Estimates of the three-dimensional flame surface
4 density and every term in its transport equation from two-dimensional measurements, *Proc.*
5 *Combust. Inst.* 33 (1) (2011) 1447–1454.
6
7 [33] T. D. Dunstan, N. Swaminathan, K. N. C. Bray, Influence of flame geometry on turbulent
8 premixed flame propagation: a DNS investigation, *J. Fluid Mech.* 709 (2012) 191–222,
9 publisher: Cambridge University Press.
10
11 [34] N. Swaminathan, R. W. Bilger, G. R. Ruetsch, Interdependence of the Instantaneous Flame
12 Front Structure and the Overall Scalar Flux in Turbulent Premixed Flames, *Combust. Sci.*
13 *Technol.* 128 (1997) 73–97.
14
15 [35] N. A. Worth, T. B. Nickels, N. Swaminathan, A tomographic PIV resolution study based
16 on homogeneous isotropic turbulence DNS data, *Exp. Fluids* 49 (3) (2010) 637–656.
17
18 [36] F. C. Gouldin, An application of fractals to modeling premixed turbulent flames, *Combust.*
19 *Flame* 68 (3) (1987) 249–266.
20
21 [37] F. C. Gouldin, S. M. Hilton, T. Lamb, Experimental evaluation of the fractal geometry of
22 flamelets, *Symp. (int.) Combust.* 22 (1) (1989) 541–550.
23
24 [38] F. C. Gouldin, K. N. C. Bray, J.-Y. Chen, Chemical closure model for fractal flamelets,
25 *Combust. Flame* 77 (3-4) (1989) 241–259.
26
27 [39] G. L. North, D. A. Santavicca, The fractal nature of premixed turbulent flames, *Combust.*
28 *Sci. Technol.* 72 (4-6) (1990) 215–232.
29
30 [40] O. L. Gulder, Turbulent premixed combustion modelling using fractal geometry, *Symp.*
31 *(int.) Combust.* 23 (1991) 835–842.
32
33 [41] N. Peters, *Turbulent Combustion*, Cambridge University Press, Cambridge, 2000.
34
35 [42] E. Giacomazzi, C. Bruno, B. Favini, Fractal modelling of turbulent combustion, *Combust.*
36 *Theory Model.* 4 (4) (2000) 391–412.
37
38 [43] E. Giacomazzi, V. Battaglia, C. Bruno, The coupling of turbulence and chemistry in a
39 premixed bluff-body flame as studied by LES, *Combust. Flame* 138 (2004) 320–335.
40
41 [44] N. K. Aluri, S. P. R. Muppala, F. Dinkelacker, Substantiating a fractal-based algebraic
42 reaction closure of premixed turbulent combustion for high pressure and the lewis number
43 effects, *Combust. Flame* 145 (4) (2006) 663–674.
44
45 [45] E. Giacomazzi, F. R. Picchia, N. Arcidiacono, D. Cecere, F. Donato, B. Favini, Unsteady
46 simulation of a CO/H₂/N₂/air turbulent non-premixed flame, *Combust. Theory Model.*
47 12 (6) (2008) 1125–1152.
48
49 [46] E. R. Hawkes, O. Chatakonda, H. Kolla, A. R. Kerstein, J. H. Chen, A petascale direct
50 numerical simulation study of the modelling of flame wrinkling for large-eddy simulations
51 in intense turbulence, *Combust. Flame* 159 (8) (2012) 2690–2703.
52
53 [47] F. Cavallo Marincola, T. Ma, A. M. Kempf, Large eddy simulations of the Darmstadt
54 turbulent stratified flame series, *Proc. Combust. Inst.* 34 (1) (2013) 1307–1315.
55
56
57
58
59
60
61
62
63
64
65

1
2
3
4
5
6
7
8
9
10
11
12
13
14
15
16
17
18
19
20
21
22
23
24
25
26
27
28
29
30
31
32
33
34
35
36
37
38
39
40
41
42
43
44
45
46
47
48
49
50
51
52
53
54
55
56
57
58
59
60
61
62
63
64
65

[48] R. Keppeler, E. Tangermann, U. Allaudin, M. Pfitzner, LES of Low to High Turbulent Combustion in an Elevated Pressure Environment, *Flow, Turbul. Combust.* 92 (3) (2014) 767–802.

[49] Y. Gao, N. Chakraborty, N. Swaminathan, Algebraic Closure of Scalar Dissipation Rate for Large Eddy Simulations of Turbulent Premixed Combustion, *Combust. Sci. Technol.* 186 (10-11) (2014) 1309–1337.

1
2
3
4
5
6
7
8
9
10
11
12
13
14
15
16
17
18
19
20
21
22
23
24
25
26
27
28
29
30
31
32
33
34
35
36
37
38
39
40
41
42
43
44
45
46
47
48
49
50
51
52
53
54
55
56
57
58
59
60
61
62
63
64
65